Electric-field stabilized vortex nematicons in low-birefringent nematic liquid crystals

Michał Kwaśny*, Mirosław Karpierz and Urszula Laudyn

Faculty of Physics, Warsaw University of Technology, Koszykowa 75, 00-662 Warszawa,

Received December 05, 2025; accepted December 29, 2025; published December 31, 2025

Abstract—We report on the generation and electric-field stabilization of scalar vortex nematicons in a low-birefringence nematic liquid crystal (LB NLCs). Using mixture 903, we demonstrate self-confined vortex beams that preserve their topological charge and maintain a doughnut-shaped profile over millimetre-scale distances. Utilizing a low-frequency electric field, we show that temporal fluctuations, polarization mixing, and azimuthal distortions are substantially reduced. Interferometric measurements confirm the presence of robust phase singularities, while intensity maps reveal enhanced symmetry and stability as the voltage increases. The combined effects of LB and electric-field-induced fluctuation quenching establish the 903 NLCs mixture as a promising platform for stable vortex spatial solitons and tunable structured-light photonic applications.

Vortex beams (VBs), characterized by an azimuthally symmetric phase profile and a phase singularity on axis, offer unique opportunities for optical trapping, particle manipulation, quantum information encoding, and high-capacity data transmission. When these structured beams propagate in self-focusing nonlinear media, they can form self-localized wavepackets – vortex solitons – in which nonlinear index changes dynamically balance diffraction [1–4]. Nematic liquid crystals (NLCs) are particularly attractive in this context, as reorientational nonlinearities provide a strong and highly nonlocal response. Over the past two decades, extraordinarily polarized spatial solitons in NLCs – nematicons – have been extensively investigated [5–7]. They arise from light-induced molecular reorientation, which creates a graded refractive index profile. The resulting nonlocality, similar to that of thermal media [8–10], leads to enhanced stability, robustness, bistability, and long-range interactions in self-confined beams [11]. More recently, attention has shifted from Gaussian beams to structured light in NLCs. Airy beams in NLCs have been shown to undergo power-dependent localization and soliton formation, including the generation of off-shoot solitons [12]. The VBs have been used to form "vortex nematicons" (VNs) in planar cells, although their strong tendency to azimuthal breakup has been recognized for a long time [13–15]. It is now understood that, unless the optical anisotropy is sufficiently small [13, 17], birefringence-induced anisotropic diffraction breaks the degeneracy of underlying dipole-like modes and drives structural instability. Consistently, experiments have demonstrated that LB or moderate-birefringence mixtures support stable charge-one VNs over millimetre-scale distances. In contrast, standard high-birefringence (HB) compounds display pronounced temporal and structural instabilities. The fluid nature of NLCs leads to long-range correlated director fluctuations, manifesting as slow random walks and breathing of self-trapped beams. Several strategies have been proposed to minimise such fluctuations, including partial photopolymerization [18] and the application of low-frequency (LF) electric fields to negative dielectric anisotropic NLCs [19, 20]. Despite these advances, the combined actions of LB and electric-field-induced fluctuation quenching on scalar VNs remain unaddressed. Currently, field-assisted stabilization primarily focuses on Gaussian nematicons or vortex structures bound to defects or magnetically controlled textures. It remains an open question whether a reorientationally supported scalar vortex in LB NLCs mixture can be made more robust, both structurally and temporally, by a superimposed LF electric field. Using the LB NLCs mixture, previously optimized for self-guided beams [20, 21] and Airy-beam localization [12], we generate a scalar vortex nematicon and subject it to a transverse AC electric field. We show that the applied field enhances azimuthal symmetry and suppresses temporal fluctuations of the VNs, while preserving their topological charge (TC) and guiding properties.

Experiments were performed in planar cells with a 30-μm gap, equipped with indium–tin–oxide (ITO) electrodes to apply a voltage along the *x*-axis. A polyimide alignment layer rubbed unidirectionally at an approximate 45° angle with respect to the optical *z*-axis imposed homogeneous planar anchoring of the director in the *yz*-plane. The analyzed propagation distance was about 2 mm, which is comparable to the lengths used in previous nematic and vortex-nematic experiments. The cell was filled by capillary action with the LB 903 NLC [22], characterized by ordinary and extraordinary refractive indices $n_o \approx 1.47$

* E-mail: michal.kwasny@pw.edu.pl

and $n_e \approx 1.54$ at 1064nm. It also exhibits negative dielectric anisotropy at a LF of 1kHz, i.e. with dielectric susceptibilities $\epsilon_\parallel < \epsilon_\perp$ along and across $\boldsymbol{n}$, respectively $(\epsilon_\parallel - \epsilon_\perp = -1.34)$

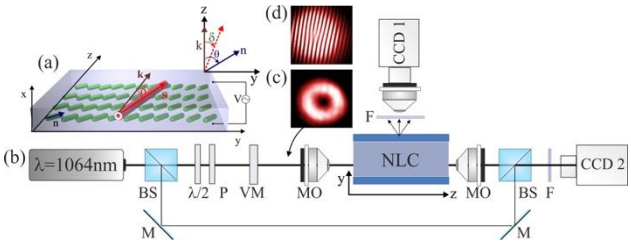

Fig. 1. (a)-(b) Geometry of the planar NLC cell and sketch of the experimental setup showing the coordinate system, director orientation, applied electric field, and the vortex beam launched at the mid-plane: BS – beam splitter, $\lambda/2$ – half-wave plate, P – polarizer, VM – vortex mask, M – mirror, MO – microscope objective, F – pass-band filter, CCD – digital camera, NLC – liquid crystal cell. Inset (c) transverse intensity profile of the input VB and (d) its interferogram with a single fork-type dislocation confirming topological charge $\ell = 1$.

The optical excitation was provided by a CW Nd:YAG laser, as sketched in Fig. 1 ($\lambda = 1064nm$). The coupled beam was linearly polarized along the y-axis, exciting an extraordinary wave in the NLCs. A commercial vortex retarder (Thorlabs) converted the fundamental Gaussian beam into a first-order azimuthally symmetric vortex with a TC of $\ell = 1$. The VB was focused with a transverse waist width of 5 μm. The beam evolution along the propagation direction (z) was tracked using a digital camera positioned above the *yz*-observation plane. At the cell exit facet (z = 2 mm) in the transverse *xy*-plane, an additional CCD camera simultaneously imaged the spatial intensity distribution and the fringe pattern resulting from a Mach-Zehnder-type interferometer to reveal the phase structure of the analysed optical field. A fork-type dislocation in the interferograms confirmed the presence and sign of the topological charge. To evaluate the temporal stability of the VN, time-series measurements were acquired at fixed power and voltage.

NLCs are mesophases in which intermolecular interactions promote orientational order despite positional randomness [23]. When anchored planarly at a rubbed polyimide interface, they behave as uniaxial media with refractive indices $n_\parallel$ (*e*-wave) and $n_\perp$ (*o*-wave) for electric an field **E** across and along the optic axis $\boldsymbol{n}$. Launching an *e*-polarized, bell-shaped beam (with the field in the plane of $\boldsymbol{n}$ and $\boldsymbol{k}$) generates a torque $\Gamma = \epsilon_0 \epsilon_a (\boldsymbol{n} \cdot \boldsymbol{E})(\boldsymbol{n} \times \boldsymbol{E})$ with $\epsilon_a = n_\parallel^2 - n_\perp^2$ being the optical anisotropy, that drives all-optical molecular reorientation, increasing the angle between $\boldsymbol{k}$ and $\boldsymbol{n}$, and thus the extraordinary effective refractive index $n_e(\theta) = n_\perp n_\parallel / (\epsilon_a + \sin^2\theta + n_\parallel^2)$. The difference $\Delta n_e^2(\theta) = n_e^2(\theta) - n_e^2(\theta_0)$ supports self-focusing and, eventually, self-confined wave packets, such as nematicons as well as vortex-nematicons. Figure 2 summarizes the generation of VNs in three nematic mixtures with decreasing birefringence: 6CHBT ($\epsilon_a = 0.4$), 903 ($\epsilon_a = 0.2$), and 1110 ($\epsilon_a = 0.1$).

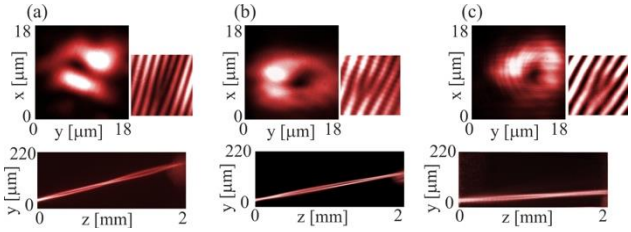

Fig. 2. VNs in NLCs of decreasing anisotropy and increasing optical powers; (a) $\epsilon_a = 0.4$, $P = 4.5mW$, (b) $\epsilon_a = 0.2$, $P = 15mW$, (c) $\epsilon_a = 0.1$, $P = 27mW$. Top panels: output intensity distribution (left) and interferogram (right), exhibiting the fork dislocation as for $\ell = 1$ TC VB. Bottom panels: propagation dynamics in the *yz*-plane.

In all samples with a thickness of 30 μm (not shown), at low input powers, the doughnut-shaped vortex broadens, and its peak intensity decreases along z, as expected from linear diffraction. At milliwatt power levels (roughly 4.5 mW for 6CHBT NLC, 11 mW for 903 NLC, and 27 mW for 1110 NLC), a self-confined doughnut-shaped structure emerges, maintaining its transverse profile throughout the cell length and preserving the on-axis phase singularity, as evidenced by a stable fork dislocation in the interferograms. The HB mixture 6CHBT exhibits a markedly distorted intensity profile: the ring is asymmetrical and deviates from the typical doughnut shape, indicating the onset of vortex breakup, even though the phase singularity remains visible. In contrast, the intermediate- and low-birefringence mixtures 903 and 1110 display symmetric, ring-like intensity distributions. They also display clean fork dislocations, clearly consistent with stable vortex nematicons. These observations align with previous reports that low optical anisotropy enhances vortex stability by reducing anisotropic diffraction and astigmatism [13,17]. On this basis, the subsequent analysis focuses on a 903 NLC mixture as a compromise between sufficiently low birefringence for stability and sufficiently strong nonlinearity at moderate powers.

Since the 903 NLCs exhibits $\Delta\epsilon < 0$ at low frequencies, the Γ can also describe the electro-optic response of the medium, that can be obtained by replacing $(n_\parallel^2 - n_\perp^2)$ with $(\epsilon_\parallel - \epsilon_\perp)$ and the field $\boldsymbol{E}$ with the low-frequency field $\boldsymbol{E}_{lf}$ corresponding to an applied voltage. For an external voltage applied across the cell thickness (the *x*-direction), the director tilts away from the field vector, effectively reducing the average pretilt angle relative to the substrates and quenching director fluctuations, as previously established in electro-optic studies and nematicon fluctuation-quenching experiments [19, 20].

Figure 3 shows the temporal evolution maps of the vortex nematicon at the output of a 30-μm-thick 903 cell for applied voltages of 0, 20, and 50 V. Each panel displays a time sequence of intensity profiles together with the corresponding interferograms. At 0 V, the vortex nematicon exhibits noticeable temporal fluctuations, with asymmetries and local intensity peaks evolving in time,

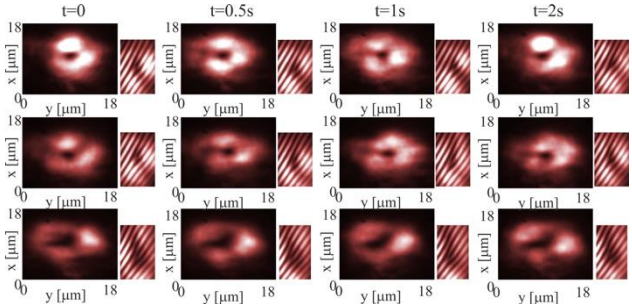

Fig. 3. Time sequence (as marked above photos) of a vortex-nematicon at the output plane (propagation at z=2mm) in 903 NLC for increasing voltage (a) V=0, (b) V=20V, (c) V=50V. The fringe patterns are shown beside the corresponding intensity distributions.

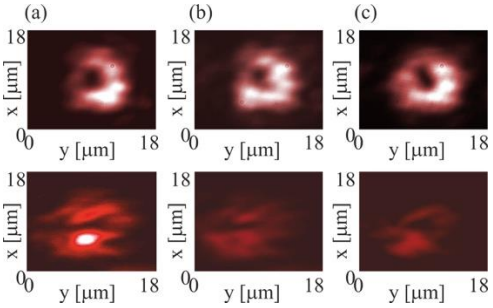

Fig. 4. The output field of the vortex nematicon in a 903 NLCs mixture imaged with an analyzer. Upper row: TE (e-wave) component; Lower row: TM (o-wave) component for (a) V=0V, (b) V=20V, (c) V=50V.

although the phase singularity persists. When a 20 V bias is applied, the temporal drift is reduced, and the ring becomes more symmetric. At 50 V, the output pattern is nearly stationary: the intensity distribution is smooth and uniform, while the interferograms confirm a stable, well-defined fork dislocation throughout the sequence.

To further elucidate the role of the electric field, Fig. 4 shows polarization-resolved output patterns obtained with an analyzer in front of the camera, enabling the separate detection of the *e*-wave (TE) and *o*-wave (TM) components. At 0 V, a substantial TM component is present alongside the dominant TE field, indicating polarization mixing during propagation. This parasitic *o*-wave contribution affects both the intensity distribution and the stability of the generated vortex soliton. At higher voltages (20 V and 50 V), the TM component becomes negligible, and the TE component's intensity profile becomes more uniform and symmetric.

For vortex nematicons, the impact of fluctuation quenching is twofold. First, reducing random variations of local birefringence prevents distortions of the nonlocal index, which well balances diffraction and nonlinearity—an interaction required for stable vortex propagation. Second, maintaining the extraordinary polarization state throughout the cell suppresses accidental excitation of the *o*-wave component and associated geometric-phase effects, which are known to perturb nematicon-guided beams and structured-light propagation in anisotropic media. As a result, the electrically stabilized vortex nematicon in 903 combines the structural robustness provided by LB with the temporal stability achieved through electric-field-induced fluctuation quenching.

We have experimentally demonstrated scalar VNs in NLCs and shown that their stability can be significantly enhanced by combining low birefringence with a low-frequency external electric field. A transverse AC bias suppresses temporal fluctuations and polarization mixing while preserving the phase singularity and guiding properties. This approach provides a robust and tunable platform for structured light propagation, with applications in vortex waveguiding, optical trapping, and topological photonics.

This work was supported by POB FOTECH of Warsaw University of Technology within the Excellence Initiative Research University (IDUB) programme.

References

[1] W.J. Firth, D.V. Skryabin, Phys. Rev. Lett. **79**, 2450 (1997).
[2] Y.V. Izdebskaya, A.S. Desyatnikov, G. Assanto, Y.S. Kivshar, Opt. Expr. **19**, 21457 (2011).
[3] Y.V. Izdebskaya, V.G. Shvedov, P.S. Jung, W. Krolikowski, Opt. Lett. **43**(1), 66 (2018).
[4] Z. Xu, N.F. Smyth, A.A. Minzoni, Y.S. Kivshar, Opt. Lett. **34**(9), 1414 (2009).
[5] G. Assanto, M.A. Karpierz, Liq. Cryst. **36**(10), 1161 (2009).
[6] M. Peccianti, G. Assanto, Phys. Rep. **516**, 147 (2012).
[7] G. Assanto, Liq. Cryst. Rev. **6**(2), 170 (2018).
[8] G. Vitrant, R. Reinisch, J.Cl. Paumier, G. Assanto, G.I. Stegeman, Opt. Lett. **14**(16), 898 (1989).
[9] C. Rotschild, O. Cohen, O. Manela, M. Segev, T. Carmon, Phys. Rev. Lett. **95**(21), 213904 (2005).
[10] S. Skupin, O. Bang, D. Edmundson, W. Krolikowski, Phys. Rev. E **73**(6), 066603 (2006).
[11] N. Smyth, A. Piccardi, A. Alberucci, G. Assanto, J. Nonl. Opt. Phys. Mat. **25**(4), 1650043 (2017).
[12] M. Kwasny, D. Hertsch, U. Laudyn, Opt. Lett. 49 (20), 5905 (2024).
[13] U. Laudyn, M. Kwasny, M. Karpierz, G. Assanto, Opt. Expr. 28, 8282 (2020).
[14] M. Kwasny, M. Karpierz, G. Assanto, U. Laudyn, Opt. Lett. **45**, 2451 (2020).
[15] A.A. Minzoni, N.F. Smyth, Z. Xu, and Y.S. Kivshar, Phys. Rev. A **79**, 063808 (2009).
[16] G. Assanto, A.A. Minzoni, N.F. Smyth, Opt. Lett. **39**(3), 509 (2014).
[17] P.S. Jung, Y. Izdebskaya, V.G Shvedov, D.N Christodoulides, W. Krolikowski, Opt. Lett. **46**(1), 62 (2021).
[18] N. Karimi, A. Alberucci, M. Virkki, A. Priimägi, M. Kauranen, G. Assanto, Photon. Lett. Pol. **8** (1), 2 (2016).
[19] J.F. Henninot, J.F. Blach, M. Warenghem, J. Opt. A: Pure Appl. Opt. **10**, 085104 (2008).
[20] U. Laudyn, M. Kwasny, M. Karpierz, G. Assanto, Opt. Lett. **44**(1), 167 (2019).
[21] M. Kwasny, U.A. Laudyn, F.A. Sala, A. Alberucci, M.A. Karpierz, G. Assanto, Phys. Rev. A **86**(1), 01382 (2012).
[22] B. Klus, U.A. Laudyn, M.A. Karpierz, B. Sahraoui, Opt. Expr. **22**(24), 30257 (2014).
[23] I.C. Khoo, Phys. Rep. **471**, 221 (2009).